Evaluation of the SAFT-γ Mie force field with solvation free energy calculations

Isabela Q. Matos and Charlles R. A. Abreu*

School of Chemistry, Federal University of Rio de Janeiro, Av. Athos da Silveira Ramos 149, Rio de Janeiro,RJ 21941-909, Brazil

E-mail: *abreu@eq.ufrj.br

Abstract

We, at this work, studied the solvation free energy differences of molecules mimicking asphaltenes in different solvents with the SAFT-γ Mie force field. We obtained solvation free energy differences by carrying out molecular dynamics simulations at the expanded ensemble. The output from these simulations was then used to estimate the differences with the MBAR method. The results with solvents other than water had low absolute deviations to the experimental data. Meanwhile, the hydration free energy calculations required a binary interaction parameter estimated with output data from molecular dynamics in order to obtain accurate free energy differences. These results indicated some problems on the SAFT-γ Mie model for water, but, generally, proved that this coarse-grained model could represent the free energy differences of the studied sets of solute-solvent.

Introduction

Solvation free energy calculations with molecular dynamics (MD) have a variety of applications ranging from drug design in the pharmaceutical industry to the development of separation technologies in the chemical industry. Solvation free energy is, more specifically, the difference in free energy related to the process of transferring the solute from the ideal gas phase condition to the liquid solvent phase condition[1]. Through the study of the solvation phenomenon, it is possible to obtain information about the behavior of the solvent in different chemical environments and the influence of the solute's molecular geometry. It is also possible to calculate other important properties with the solvation free energy, namely the activity coefficient at infinite dilution, Henry constant and partition coefficients. Additionally, solvation free energy calculations can be part of the process of calculating solubility with molecular dynamics[2].

The solvation phenomenon described above is intrinsically complex. There are many competing forces interfering in the behavior of the solute-solvent interaction, and free energy simulations are susceptible to sampling problems in low energy regions. Various simulation methodologies were developed to enable estimations of energy differences such as the expanded ensemble,[3] thermodynamic integration,[4] free energy perturbation (FEP)[5–7] and umbrella sampling.[8] Utilizing FEP methodologies, recent papers[9,10] made available a big database of hydration free energy of small molecules using the GAFF force field. Beckstein et al.[11] also calculated the hydration free energies for fifty-two compounds with the OPLS-AA force field. They obtained an overall root mean square deviation to the experimental data of 1.75 kcal/mol and concluded that the reproducibility of the Lennard-Jones parameters main limiter of the precision of the results. A comparison of polar and nonpolar contributions to

these hydration free energies indicated the significance of each the terms.[12] Garrido et al.[13,14] calculated the free energy of solvation of large alkanes in 1-octanol and water with three different force fields (TraPPE, GROMOS, OPLS-AA/TraPPE) and the solvation free energy of propane and benzene in non aqueous solvents like n-hexadecane, n-hexane, ethylbenzene, and acetone with the force fields TraPPE-UA and TraPPE-AA. Roy et al.[15] addressed the choice of the Lennard Jones parameters for predicting solvation free energy in 1-octanol. They calculated the solvation free energy of a set of 205 small organic molecules in 1-octanol and found that the force field parametrization of n-octanol proposed by Kobryn and Kovalenko[16] provided the best agreement. Gonçalves and Stassen[17] calculated the free energy of solvation using the polarizable continuum model coupled to molecular dynamics computer simulation with the GROMOS force field. These calculations were done with a representative set of solutes and with the solvents tetrachloride, chloroform, and benzene. Using the GAFF and the polarizable AMOEBA force fields, Mohamed et al.[18] evaluated the solvation free energy of small molecules in toluene, chloroform, and acetonitrile, and obtained a mean unsigned error of 1.22 kcal/mol for AMOEBA and 0.66 kcal/mol for GAFF. To define the role of solvent water in the docking structure determination of proteins, Matubayasi[19] developed a method to compute the solvation free energy of proteins while using OPLS-AA force field for the solutes and TIP3P for water. Genheden[20] expanded the Elba force field to calculate solvation free energies of more than 150 solutes taken from the Minnesota solvation database in polar (water, hexanol, octanol and nonanol) and apolar (hexane, octane, and nonane) solvents. They obtained mean absolute deviations of 1 kcal/mol for water and 1.5 kcal/mol for hexane. In this model, three carbons are represented by a single bead and water is represented by a single bead.

Another influencing factor in the output of these calculations is the choice of force field used to model the solvent and solute molecules. Coarse-grained force fields generally reproduce free energy differences since the effects of reducing degrees of freedom in the entropy are counterbalanced by the reduction of enthalpic terms.[21] Additionally, the success of a coarse-grained force field is essential to decrease the computational time of solvation free energy calculations and to reveal deficiencies in the description of small molecules by these models.[1,22] Hence, we, in this study, assess the efficiencies and shortcomings of the SAFT-γ Mie coarse-grained force field[23] with free energy calculations for a variety of pairs solute-solvent. This force field was chosen because it uses, unlike the majority of the force fields, the Mie potential and because its method of obtaining parameters is more straightforward than other models. It was initially parameterized with pure component equilibrium and interfacial tension data,[23] and this strategy has provided satisfactory results. Examples include the prediction of phase equilibrium of aromatic compounds, alkanes, light gases, and water,[24–26] thermodynamic properties of carbon dioxide and methane,[27] multiphase equilibrium of mixtures of water, carbon dioxide, and n-alkanes,[28] and water/oil interfacial tension.[29]

The solvents and solutes in our free energy calculations were picked to test the force field with standard sets used as a benchmark in solvation free energy calculations and with aromatic substances used as a model to asphaltenes. Asphaltenes are complicated to characterize by determining their composition on a molecular basis, but the literature broadly accepts that they can be described as a fraction of crude oil soluble in toluene and insoluble in n-alkenes (pentane, hexane, heptane).[30] They have motivated many studies with interest in developing models for their structure and behavior due to all the problems they can cause during their transportation and refining such as precipitation during the oil processing.[31] This precipitation issue is a recurrent problem due to the growing market of the production of crude oil in deep waters, which have conditions favorable to precipitation, such as pressure depletion and acid stimulation.[32] As an example, asphaltene precipitation due to pressure drop can clog oil production equipment and cause an

almost exponential increase in the cost of production.[32,33] All these factors make the understanding of the behavior of asphaltenes in different chemical and physical environments relevant to the oil industry.

As said in the previous paragraph, asphaltene characterization still faces some issues. Hence, we choose to use polycyclic aromatic hydrocarbons (PAH'S), which have well-defined characteristics, to initially test the efficiency of the SAFT-γ Mie force field in describing the solvation phenomenon. The ones utilized in this work were phenanthrene, anthracene, and pyrene since they have similarities with asphaltenes regarding their solubility. Meanwhile, we selected compounds that are used to characterize asphaltenes (toluene, hexane) as solvents in our free energy calculations. We also tested the anti-solvent/solvent effect of carbon dioxide due to its influence in asphaltene precipitation during the oil processing.[34] With this study of solvation free energies with the SAFT-γ Mie model, we intend to improve this force field and provide accurate free energy calculations of PAH's with a coarse-grained model. The correct description of these smaller asphaltene-like compounds by this force field opens up the possibility of obtaining satisfactory results for more complex asphaltene models with a less computational expensive force filed.

Computational Methods

SAFT-γ Mie Force Field

The SAFT-γ Mie is a force field that uses a coarse-graining top-down methodology in its parameterization.[23] This methodology aims to obtain the intermolecular parameters from macroscopic experimental data like fluid-phase equilibrium or superficial tension data. The idea is that the force field's parameters estimated with the equation of state SAFT-VR Mie[35] can be used on molecular simulations since both the EoS and the force field use the Mie attractive and repulsive potential:

$$U_{Mie}(r) = \epsilon \frac{\lambda_r}{\lambda_r - \lambda_a} \left(\frac{\lambda_r}{\lambda_a}\right)^{\left(\frac{\lambda_a}{\lambda_r - \lambda_a}\right)} \left[\left(\frac{\sigma}{r}\right)^{\lambda_r} - \left(\frac{\sigma}{r}\right)^{\lambda_a}\right] \quad (1)$$

The parameter ϵ is the potential well depth, σ is the segment diameter, r is the distance between the spherical segments, λ_r is the repulsive exponent and λ_a is the attractive exponent. This force field has already been successfully parameterized for a variety of fluids, and its success can be imputed to the flexibility of Mie Potential to represent the properties of real fluids.[24,25,36] Each substance has the four parameters of Eq. (1) plus the number of segments (m_s) to be estimated. However, the number of segments is usually fixed in an integer value so it can be used in coarse-grained simulations, the attractive parameter can also be fixed in the London value of 6 since there is a high correlation between the attractive and repulsive parameter.[37] There are two strategies to obtain these parameters: one is by fitting the Saft-Vr Mie Eos to experimental data as vapor pressure and liquid density,[38] and the other one is by using correspondent state parametrization.[39] In the present work, the first strategy was used to find the parameters for phenanthrene with vapor-liquid equilibrium data[40,41] following the methodology proposed by Müller and Mejía.[25] We chose to model the phenanthrene molecule with five beads and with the geometry in Figure 1, since this level of coarse-graining was also used for a similar molecule (anthracene) in the original paper.

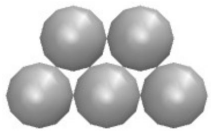

Figure 1: Geometry for $m_s = 5$.

The parameter for the other compounds were retrieved from the literature, and all these parameters are exposed in Table 1. For a mixture, the mixing rules used on can be seen on Eqs. (2), (3) and (4)[35] .

$$\sigma_{ij} = \frac{\sigma ii + \sigma jj}{2} \quad (2)$$

$$\lambda_{k,ij} - 3 = \sqrt{(\lambda_{k,ii} - 3)(\lambda_{k,jj} - 3)}, k = r, a \quad (3)$$

$$\epsilon_{ij} = (1 - k_{ij}) \frac{\sqrt{\sigma_{ii}^3 \sigma_{jj}^3}}{\sigma_{ij}^3} \sqrt{\epsilon_{ii}\epsilon_{jj}} \quad (4)$$

After the first estimations, we realized the need to estimate the binary interaction parameter of Eq. 4 for pairs with water as a solvent. Hence, we estimated k_{ij} for these pairs and, for all the other pairs, we set k_{ij} to zero. The estimation was done by performing trial expanded ensemble simulations in three values of the parameter, as suggested by Ervik et al..[42] With the ΔG_{solv} obtained with these simulations, we did a linear fit to acquire the refined value of the parameter. We used this strategy because the estimation with SAFT VR Mie EoS gave poor results for the solvation free energies.

Table 1: SAFT-γ Mie Force Field for each substance used in this work.

	m_s	ϵ/k_B (K)	$\sigma(\dot{A})$	λ_r
Water[28]	1	305.21	2.902	8.0
Propane[24]	1	426.08	4.871	34.29
Carbon dioxide[24]	2	194.94	2.848	14.65
Hexane[24]	2	376.35	4.508	19.57
Octanol[36]	3	495.71	4.341	28.79
Toluene[25]	3	268.24	3.685	11.80
Benzene[25]	3	230.30	3.441	10.45
Pyrene[25]	4	459.04	4.134	15.79
Anthracene[25]	5	259.68	3.631	9.55
Phenanthrene	5	262.74	4.077	9.55

Expanded Ensemble

The strategy chosen in this work to calculate the solvation free energy differences was to use an alchemical method in which the solute molecule is gradually inserted in the solvent using a thermodynamic cycle.[43] Each insertion or alchemical state is represented by a coupling parameter, λ, that ranges from 0 to 1. When $\lambda = 0$, there is no interaction with the solvent and, when $\lambda = 1$, the interactions are fully activated. Since the force field used does not explicitly take in consideration the charges, the interactions are only due to the Mie potential. The coupling of the Mie Potential is done non linearly through the generalization of the soft-core potential[44] :

$$U_{Mie}^{sc}(r) = \lambda\epsilon \frac{\lambda_r}{\lambda_r - \lambda_a} \left(\frac{\lambda_r}{\lambda_a}\right)^{\left(\frac{\lambda_a}{\lambda_r - \lambda_a}\right)} \left\{ \frac{1}{[\alpha(1-\lambda) + (r/\sigma)^{\lambda_a}]^{\lambda_r/\lambda_a}} - \frac{1}{\alpha(1-\lambda) + (r/\sigma)^{\lambda_a}} \right\} \quad (5)$$

Here, α is a constant in which the value of 0.5 is normally assumed to it. Instead of doing various simulations in different values of λ, we decided to carry out expanded ensemble simulations.[3] This methodology was developed in order to allow the sampling of different states in only one simulation. The statistical expanded ensemble, Z can be defined as a sum of sub ensembles Z_i in different values of λ:

$$Z = \sum_{i=1}^{N} Z_i exp(\eta_i) \quad (6)$$

where N is the number of alchemical states and η_i is the arbitrary weight of the sub ensemble Z_i at each state. These weights allow the sampling of the states during the simulation. A sufficient number of states needs to be sampled in order to obtain the solvation free energies differences between two end states ($G_i - G_j$) from the simulations' results. The weights are calculated doing series of trial simulations following the flat-histogram approach.[45–47] For the first simulation, the values of η are chosen arbitrarily or they are set to zero and, with the outcome form this simulation, the histogram of the states visited is obtained. This histogram is then used to estimate the free energy differences and, since the weights are related to the free energies by Eq. (7)), the next values of η. This iteration goes on until a uniform distribution is secured.

$$(\eta_i - \eta_j)_{k+1} = \beta(G_i - G_j)_k \quad (7)$$

The final weights can then be used in a longer simulation to obtain the total potential energies for the solvation free energy calculations. In the present work, the Multistate Bennett Acceptance Ratio (MBAR)[7] method was used to obtain this free energy differences, this method requires that data are uncorrelated so an additional subsampling is necessary. The values of lambda were optimized using the method developed by Escobedo and Martinez-Veracoechea[48] to decrease the round trip time. The method uses the fraction of times that the trial simulation at state λ_i has most recently visited the state $\lambda = 1$ as opposed to state $\lambda = 0$ to obtain the optimized group of λ to be used in the final simulation.

Molecular Dynamic Simulations

Using the parameters for phenanthrene estimated and the available SAFT-γ Mie force field parameters, we carried out molecular dynamic simulations to estimate solvation free energy differences. The chosen software package to perform the simulations was the Lammps package.[49] In it, the motion equations were integrated with the velocity-Verlet algorithm[50] with a time step of 2 fs. As required by the coarse-grained model, molecules were treated as rigid bodies. The thermostat and the barostat were the Nose/Hoover with chains with damping factors of 100 and 1000 time steps respectively. Electrostatics interactions are not explicitly accounted by the SAFT-γ Mie force field, hence there were no shifting of forces or long-range corrections. The potential cutoff was equal to 20 $\dot{A}$[25] with a neighbor skin of 2 $\dot{A}$. The initial configurations of the solvated systems were generated using the Playmol package.[51] For the binary mixtures, one molecule of solute and a varying number of solvent molecules- 700 molecules of toluene, 700 molecules of octanol, 1024 molecules of hexane, 3000 molecules of water - were randomly added to a cubic box. We did the simulations to study solvation free energy of phenanthrene in a mixture of toluene and carbon dioxide with different weight fractions of carbon dioxide. The system consisted of one molecule of phenanthrene for all the fractions and 123 molecules of CO_2 and 618 molecules of toluene for $w_{CO_2} = 0.087$; 166 molecules of CO_2 and 589 molecules of toluene for $w_{CO_2} = 0.119$; 232 molecules of CO_2 and 545 molecules of toluene for $w_{CO_2} = 0.169$; 380 molecules of CO_2 and 446 molecules of toluene for $w_{CO_2} = 0.289$.

All simulations were performed with the constant temperature and pressure values of 298 K and 1 bar, except the ones containing carbon dioxide. These had the temperature of 298 K and the pressure of the liquid phase equilibrium correspondent to the CO_2 fraction.[52] For all the simulations, the initial box was equilibrated at the NPT ensemble for two ns, and the resulting configurations were used as the initial configuration of the expanded ensemble simulations. These were carried out with the Lammps user package for expanded ensemble simulations with the Mie Potential developed by our group, available at https://github.com/atoms-ufrj/USER-ALCHEMICAL.

During these expanded ensemble simulations, the sampling of a new alchemical state was tried at every 10 MD steps. To define the optimal values of λ and η related to each state, short trials simulations, having around nine ns of production time, were carried out. In the first simulation, we chose the group of λ arbitrarily, and we set the ηs to zero, or we assigned to them the values found for similar pairs of solute-solvent. The subsequent group of η were estimated with the flat histogram approach (Eq. 7). We then did another trial simulation with the new weights. The results of this simulation were used to optimize the group of λs by minimizing the number of round trips. The ηs correspondent to the newest group of λ were interpolated linearly from the free energy differences. With the final values of η and λ defined for each mixture, larger simulations with a production time of 20 ns were carried out.

Since the force field used considers that the beads do not have charges are rigid, the total potential energy is equal to the Mie potential. The post-processing method used to effectively calculate free energy differences with the potential energies obtained from the expanded ensemble simulations was the Multistate Ben-

net Acceptance Ratio (MBAR). The software alchemical-analysis[43] was utilized to obtain the ΔG_{solv} with MBAR and to assess the quality of the results.

Results and discussion

Solvation free energies

The solvation free energies of aromatic solutes in nonpolar (hexane), aromatic (toluene) and hydrogen bonding (1-octanol) solvents were examined with binary interaction parameters equal to zero. Since the force field does not account for charges, we only needed to calculate the Mie contribution (Eq. 5) to the solvation free energy. A total of 15-18 λs, depending on the pairs solute-solvent, and their respective ηs were estimated as described in the methodology. The final λ set was found using the cumulative probability distribution for all pairs. The optimized values of λ and η can be seen in Table 2 for the hexane+benzne pair. The λs and ηs for the other pairs are available at the supporting information. Observing the coupling parameters found for all the pairs, we can see that they are concentrated on the region with a steeper slope as it is expected.

Table 2: Optimized values of λ and η for the pair benzene + hexane.

λ	η
0	0
0.065	0.708
0.112	1.385
0.15	1.892
0.188	2.399
0.226	2.519
0.264	2.457
0.304	2.367
0.356	1.921
0.411	1.411
0.492	0.524
0.588	-0.663
0.69	-2.016
0.824	-3.922
1	-6.583

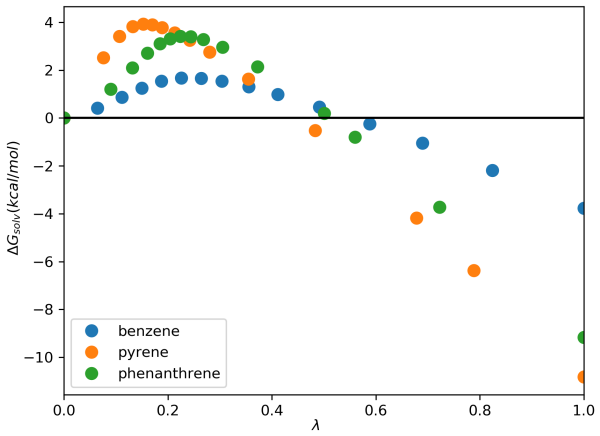

(a)

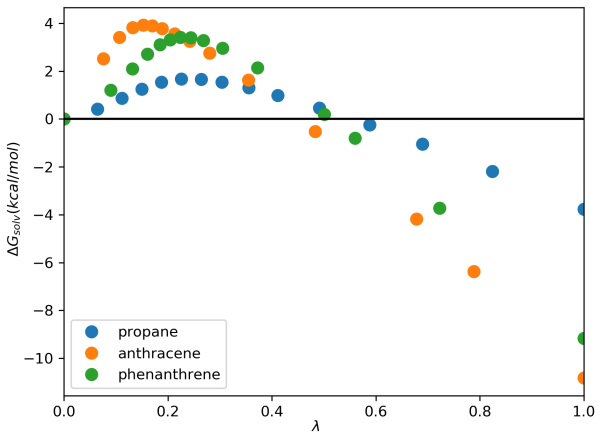

(b)

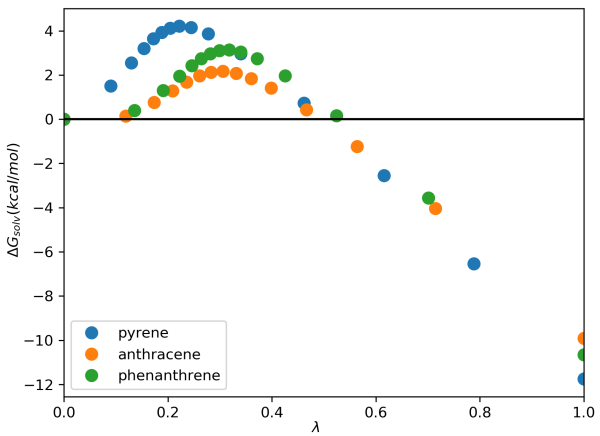

(c)

Figure 2: Solvation free energy profiles of different solutes in hexane (a), 1-octanol (b), and toluene (c).

After the expanded ensemble simulations with the intermediate states and weights es-

Table 3: Calculated and experimental values for the solvation free energy differences (kcal/mol) of solutes in non aqueous solvents.

Solvent	Solute	ΔG_{solv}^{exp}	ΔG_{solv}^{Mie}	Absolute Deviation
hexane	benzene	-3.96	-3.76 ± 0.01	0.20
hexane	pyrene	-11.53	-10.82 ± 0.02	0.71
hexane	phenanthrene	-10.01	-9.16 ± 0.01	0.85
1-octanol	propane	-1.32	-1.36 ± 0.02	0.04
1-octanol	anthracene	-11.72	-8.16 ± 0.03	3.61
1-octanol	phenanthrene	-10.22	-8.34 ± 0.03	1.47
toluene	pyrene	-12.86	-11.74 ± 0.01	1.11
toluene	anthracene	-11.31	-9.90 ± 0.01	1.41

timated, we calculated the solvation free energy differences with MBAR. These results and and the absolute deviations to experimental data[53] are available in Table 3. The numerical values for solvation free energies in hexane had smaller absolute deviations to experimental data, what shows that the SAFT-γ Mie force field performs better for a non-polar solvent. Additionally, this force field presented better results for the pair hexane+benzene than the Trappe force field (- 4.35 ± 0.05 kcal/mol)[13] and the ELBA coarse-grained force field (-2.92 ± 0.01 kcal/mol).[20] We also observed the effect of molecule's size on the entropic region of the free energy curve in Figure 2. It was expected that a force field based on an EoS that does not explicitly account for hydrogen bond would not perform well for 1-octanol. Despite this, the solvation free energies of propane and phenanthrene in 1-octanol stayed in the desired deviation range of 1-2 kcal/mol.[54] The solvation free energy absolute deviation for propane was much smaller when compared to the other solutes, what can be attributed to propane's non-polarity and smoother free energy curve (Figure 2). This solvation free energy of propane in 1-octanol also had a smaller deviation than the prediction of the ELBA force field (-0.92 ± 0.01).[20] The anthracene and phenanthrene molecules have the same geometry in the model and similar physical properties, but the absolute deviation of the solvation free energy of anthracene in 1-octanol is much higher than the one of phenanthrene 1-octanol. This high deviation may indicate a problem in the parameterization of anthracene. The results also indicated the prediction capability of the force field for pairs of aromatic solute and solvent. The influence of the molecule's geometry on the free energy curves was the same as the one observed for other solvents (Figure 2). ΔG_{solv} was also calculated for phenanthrene in toluene and in toluene+CO_2. To the best of our knowledge, there were no available experimental data for these solvation free energies, but the previous results for phenanthrene in other solvents and for the pair anthracene+toluene showed that the force field is adequate to describe the solvation phenomenon of phenanthrene in an aromatic solvent. The results for these sets are exposed in Table 4.

Table 4: Calculated values for the solvation free energy differences (kcal/mol) of phenanthrene in toluene+CO_2.

w_{CO_2}	ΔG_{solv}^{Mie}
0.0	-10.65 ± 0.02
0.087	-10.73 ± 0.02
0.119	-10.78 ± 0.02
0.169	-10.71 ± 0.02
0.289	-10.69 ± 0.02

The increase of CO_2 mass fraction in toluene caused a small effect on solvation free energies. First, the ΔG_{solv} decreased with the increase of w_{CO_2}. After the 0.119 fraction, the effect was reversed and carbon dioxide became an anti-solvent. Soroush et al.[34] reported that asphal-

tene precipitation occurs when carbon dioxide mass fractions became higher than 0.10 in the system asphaltene+toluene+carbon dioxide, what is in agreement with the anti-solvent effect of carbon dioxide observed on the calculated values. It is also important to point out that the small differences observed may indicate the insignificance of CO_2 in the solvation of phenanthrene in toluene when using the Saft-γ Mie force field. But, more studies need to be done to make a secure assertion about it since this is a qualitative study due to the lack of experimental data.

Hydration free energies

We also calculated the hydration free energies of widely studied solutes (propane, benzene) and aromatic solutes (toluene, phenanthrene) with a group of fifteen intermediate states. First, the binary interaction parameter was set to zero, but the preliminary results for hydration free energies, exposed in Table 6, had a high deviation from the experimental data.[55,56] After these results, the need for binary interaction parameters was clear. First, we estimated k_{ij} with the SAFT VR Mie EoS and experimental vapor pressure data, but this strategy also did not provide good results. Hence, we used the approach of estimating the k_{ij} with the output from solvation free energy calculations with molecular dynamics. We initially found individual values for the interaction parameter of each pair, but, since the parameters for aromatic solutes were very similar (0.148, 0.162, 0.152), we averaged these values. By doing that, we obtained a general parameter for the water+aromatic pairs:

Table 5: Binary interaction parameters employed.

Pair	k_{ij}
water + propane	0.067
water + aromatic	0.154

The relatively large k_{ij} value of the aromatic solutes can be pinned on the lack of an explicit association term in the model and on the water model itself since the force field did not need a k_{ij} for mixtures with the other hydrogen bonding solvent (1-octanol). This SAFT-γ Mie model for water[28] has two different temperature-dependent sets of parameters. The parameters utilized in this work was the one estimated with experimental interfacial tension data. Hence, we tested the binary interaction parameter for water+toluene estimated with MD interfacial data by Herdes et al..[29] Nevertheless, the result was not satisfactory and this parameter could not be transferable to the solvation free energy of toluene in water.

These issues faced by SAFT-γ Mie model are related to the problems of modeling water with a coarse-grained force field. One of the main difficulties is the choice of which water molecules are going to be represented by which specific beads since water molecules move independently and are only bound by non bonded interactions.[57,58] The SAFT-γ Mie water considers that one water molecule corresponds to one bead. This strategy only saves small simulation time, but it can predict properties at physiological temperatures unlike other more aggressive models, which consider that one bead represents various water molecules. In light of all this, the SAFT-γ Mie force field appears to be a good alternative when working close to room temperatures, but the necessity of additional parameters estimated with molecular simulation indicates problems on the model. Using these parameters, we then obtained the final hydration free energy differences presented in Table 6.

Hydration free energy differences calculated using the SAFT-γ Mie force field with $k_{ij} \neq 0$ had low absolute deviations to the experimental data, as expected since the parameters were adjusted to fit the experimental data. Comparing our results with other force fields, the root mean square error (RMSE) for the pairs tested with the SAFT-γ Mie model was 0.24, the RMSE for hydration free energy differences with the GAFF force field was 0.73,[9] and the RMSE for the ELBA coarse-grained force field was 0.44.[20] The difference in absolute deviations between the GAFF and SAFT-γ Mie force fields is significantly high for phenanthrene, hence the

Table 6: Calculated and experimental hydration free energy differences (kcal/mol) of solutes in water.

Solute	ΔG^{exp}_{solv}	ΔG^{Mie}_{solv} $k_{ij}=0$	Absolute Deviation	ΔG^{Mie}_{solv} $k_{ij}\neq 0$	Absolute Deviation
propane	2.00 ± 0.20	1.10 ± 0.01	0.90	2.01 ± 0.01	0.01
benzene	-0.86 ± 0.20	-4.45 ± 0.03	3.59	-1.12 ± 0.01	0.26
toluene	-0.83 ± 0.20	-10.98 ± 0.30	10.15	-0.84 ± 0.01	0.01
phenanthrene	-3.88 ± 0.60	-10.90 ± 0.04	7.12	-3.47 ± 0.02	0.41

coarse-grained force field with a binary parameter is preferred if the application requires a higher level of accuracy. The results also indicated that the SAFT-γ Mie Model with the binary interaction parameter performed better than the ELBA force field in modeling the solvation phenomenon of the pairs studied in this work and worst with the binary parameter equal to zero. This fact occurred despite the fact that both models have the same level of coarse-graining (one bead represents one water molecule). Hence, the choice between the two coarse-grained models is dependent on the availability and transferability of binary interaction parameters for the Mie Model. We also present, for the SAFT-γ Mie force field, the hydration free energy profiles in Figure 3. The geometry dependence on the free energy profiles is apparent as it was for the solvation free energy study in other solvents. We also observe that the hydration free energy for the first non zero λ is negative for benzene and toluene when a positive value is expected since energy is required to 'open space' in the solvent for the solute's insertion. This anomaly can be caused by numerical errors during the estimation or by another inconsistency in the force field.

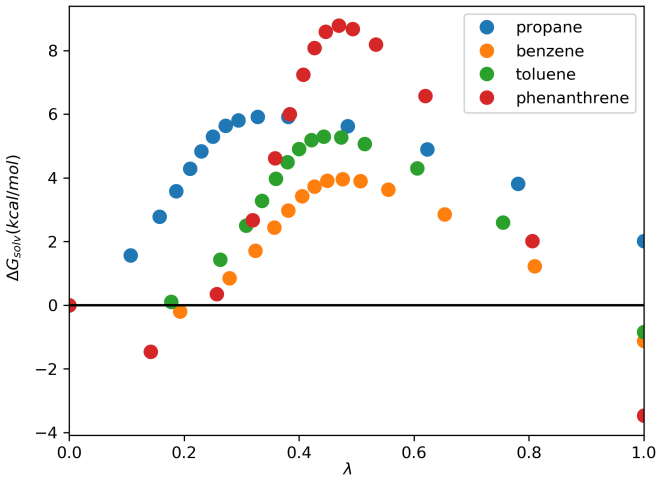

Figure 3: Hydration free energy profiles for different solutes.

Conclusions

This study consisted of solvation free energy calculations of aromatic solutes that can mimic asphaltenes in different solvents with the SAFT-γ Mie coarse-grained force field. Solvation free energy studies are mostly done using water as a solvent and with all-atom force fields based on the Lennard Jones Potential, therefore, with this study, we provided data that were lacking in the literature. Additionally, the free energy estimations done can help improve the SAFT-γ Mie force field since these calculations are helpful in identifying errors in the modeling process. The SAFT-γ Mie uses the SAFT-VR Mie EoS in its parameterization, which results in a more straightforward method of obtaining parameters. Following this strategy, the phenanthrene parameters, which were not available in this force field database, were estimated using phase equilibrium data.

To obtain accurate solvation free energies, we carefully selected and optimized the coupling parameter and their respective simulation weights used in our Expanded Ensemble simulations. The resulting potential energies from these simulations were then served as input to estimate solvation free energy differences with the MBAR method. The results for solvation free energy differences with non-aqueous solvents had absolute deviations to the experimen-

tal data of less than 2.0 kcal/mol, except for the pair 1-octanol+anthracene. We also observed the geometry effect on the free energy curves - larger molecules had steeper curves and more substantial absolute deviations. The influence of carbon dioxide on the solvation free energy of phenanthrene in toluene was found to be minimum. The ΔG_{solv} decreased slightly until the mass fraction of CO_2 was equal to 0.119 and, after this point, solvation free energies increased.

Hydration free energy differences calculations with the SAFT-γ Mie model required the use of relatively larger values of k_{ij} to obtain satisfactory results. We chose to estimate the parameter with the output from molecular dynamics data since the strategy of using the SAFT-VR Mie EoS did not provide good results. This necessity of one additional parameter happens probably due to the lack of a term to account for the hydrogen bond on the EoS that the model is based and due to the problems associated with the coarse-graining of water molecules. The results with k_{ij} estimated with MD output were great, the absolute deviations to the experimental data found were smaller than the ones for the GAFF and ELBA force field.

Overall, the SAFT-γ Mie force field proved to be an excellent model to represent the solvation phenomenon. It correctly described solvation free energy differences of solutes mimicking asphaltenes in hexane, toluene, 1-octanol, and water. The requirement of binary interaction parameter estimated with MD output for hydration free energies increases the simulation time, which is already more significant for this water model due to its coarse-graining level. Nevertheless, the SAFT-γ Mie force field for water used does not predict freezing at room temperature as other force fields, which is essential for our hydration free energy calculations.

Acknowledgement The authors thanks the financial support provided by Petrobras (project code:).

Supporting Information Available: This will usually read something like: "Experimental procedures and characterization data for all new compounds. The class will automatically add a sentence pointing to the information on-line: This material is available free of charge via the Internet at `http://pubs.acs.org/`.

References

(1) Shirts, M. R.; Pitera, J. W.; Swope, W. C.; Pande, V. S. *J. Chem. Phys.* **2003**, *119*, 5740.

(2) Schnieders, M. J.; Baltrusaitis, J.; Shi, Y.; Chattree, G.; Zheng, L.; Yang, W.; Ren, P. *J. Chem. Theory Comput.* **2012**, *8*, 1721–1736.

(3) Lyubartsev, A. P.; Martsinovski, A. A.; Shevkunov, S. V.; VorontsovVelyaminov, P. N. *J. Chem. Phys.* **1992**, *96*, 1776–1783.

(4) Kirkwood, J. *J. Chem. Phys.* **1935**, *3*, 300313.

(5) Zwanzig, R. W. *J. Chem. Phys.* **1954**, *22*, 1420.

(6) Bennett, C. *J. Comput. Phys.* **1976**, *22*, 245268.

(7) Shirts, M. R.; Chodera, J. D. *J. Chem. Phys.* **2008**, *129*, 124105.

(8) Torrie, G.; Valleau, J. *J. Comput. Phys.* **1977**, *23*, 187 – 199.

(9) Mobley, D. L.; Guthrie, J. P. *J. Comput. Aided Mol. Des.* **2014**, *28*, 711720.

(10) Matos, G. D. R.; Kyu, D. Y.; Loeffler, H. H.; Chodera, J. D.; Shirts, M. R.; ; Mobley, D. L. *J. Chem. Eng. Data* **2017**, *62*, 1559–1569.

(11) Beckstein, O.; Fourrier, A.; Iorga, B. I. *J. Comput. Aided Mol. Des.* **2014**, *28*, 265–276.

(12) Izairi, R.; Kamberaj, H. *J. Chem. Inf. Model.* **2017**, *57*, 25392553.

(13) Garrido, N. M.; Jorge, M.; Queimada, A. J.; Macedo, E. A.; Economou, I. G. *Phys. Chem. Chem. Phys* **2011**, *20*, 9155–9164.

(14) Garrido, N. M.; Queimada, A. J.; Jorge, M.; Macedo, E. A.; Economou, I. G. *J. Chem. Theory Comput.* **2009**, *5*, 2436–2446.

(15) Roy, D.; Blinov, N.; Kovalenko, A. *J. Phys. Chem. B,* **2017**, *121*, 92689273.

(16) Kobryn, A. E.; Kovalenko, A. *J. Chem. Phys.* **2008**, *129*, 134701.

(17) Gonçalves, P. F. B.; Stassen, H. *J. Chem. Phys.* **2005**, *123*, 214109.

(18) Mohamed, N. A.; Bradshaw, R. T.; Essex, J. W. *J. Comput. Chem.* **2016**, *37*, 2749–2758.

(19) Matubayasi, N. *Curr. Opin. Struct. Biol.* **2017**, *43*, 45 – 54.

(20) Genheden, S. *J. Chem. Theory Comput.* **2016**, *12*, 297–304.

(21) Kmiecik, S.; Gront, D.; Kolinski, M.; Wieteska, L.; Dawid, A. E.; Kolinski, A. *Chem. Rev.* **2016**, *116*, 78987936.

(22) Mobley, D. L.; Dumont, E.; Chodera, J. D.; Dill, K. A. *J. Chem. Phys. B* **2007**, *111*, 2242–2254.

(23) Avendaño, C.; Lafitte, T.; Galindo, A.; Adjiman, C. S.; Jackson, G.; Muller, E. A. *J. Phys. Chem. B* **2011**, *115*, 11154–11169.

(24) Herdes, C.; Totton, T. S.; Müller, E. A. *Fluid Phase Equilib.* **2015**, *406*, 91–100.

(25) Müller, E. A.; Mejía, A. *Langmuir* **2017**, -, AL.

(26) Lobanova, O.; Avendaño, C.; Lafitte, T.; Müller, E. A.; Jackson, G. *Mol. Phys.* **2015**, *113*, 12281249.

(27) Aimoli, C. G.; Maginn, E. J.; Abreu, C. R. *Fluid Phase Equilib.* **2014**, *368*, 80–90.

(28) Lobanova, O.; Mejía, A.; Jackson, G.; Müller, E. A. *J. Chem. Thermodyn.* **2016**, *93*, 320–336.

(29) Herdes, C.; Ervik, A.; Mejía, A.; Müller, E. A. *Fluid Phase Equilib.* **2017**,

(30) Sjöblom, J.; Aske, N.; Auflem, I. H.; ystein Brandal,; Havre, T. E.; ystein Sther,; Westvik, A.; Johnsen, E. E.; Kallevik, H. *Adv. Colloid Interface Sci.* **2003**, *100-102*, 399 – 473.

(31) Sjöblom, J.; Simon, S.; Xu, Z. *Adv. Colloid Interface Sci.* **2015**, *218*, 1 – 16.

(32) Buenrostro-Gonzalez, E.; Lira-Galeana, C.; Gil-Villegas, A.; Wu, J. *AIChE J.* **2004**, *50*, 2552–2570.

(33) Joshi, N. B.; Mullins, O. C.; Jamaluddin, A.; Creek, J.; McFadden, J. *Energy Fuels* **2001**, *15*, 979–986.

(34) Soroush, S.; Straver, E. J.; Rudolph, E. S. J.; Peters, C. J.; de Loos, T. W.; Zitha, P. L.; Vafaie-Sefti, M. *Fuel* **2014**, *137*, 405 – 411.

(35) Lafitte, T.; Apostolakou, A.; Avendano, C.; Galindo, A.; Adjiman, C. S.; Muller, E. A.; Jackson, G. *J. Chem. Phys.* **2013**, *139*, 154504.

(36) Ervik, A.; Mejía, A.; Müller, E. A. *J. Chem. Inf. Model.* **2016**, *56*, 1609–1614.

(37) Ramrattan, N.; Avendaño, C.; Müller, E.; Galindo, A. *Mol. Phys.* **2015**, *113*, 1–16.

(38) Avendaño, C.; Lafitte, T.; Adjiman, C. S.; Galindo, A.; Muller, E. A.; Jackson, G. *J. Phys. Chem. B* **2013**, *117*, 2717–2733.

(39) Mejía, A.; Herdes, C.; Müller, E. A. *Ind. Eng. Chem. Res.* **2014**, *53*, 4131–4141.

(40) Mortimer, S.; Murphy, R. *Ind. Eng. Chem. Res.* **1923**, *14*, 1140–1142.

(41) Osborn, A. G.; Douslin, D. R. *J. Chem. Eng. Data* **1975**, *20*, 229–231.

(42) Ervik, A.; Lysgaard, M. O.; Herdes, C.; Jiménez-Serratos, G.; MÏller, E. A.; Munkejord, S. T.; Müller, B. *J. Comput. Phys* **2016**, *327*, 576–611.

(43) Klimovich, P. V.; Shirts, M. R.; Mobley, D. L. *J. Comput. Aided Mol. Des.* **2015**, *29*, 397–411.

(44) Beutler, T. C.; Mark, A. E.; van Schaik, R. C.; Gerber, P. R.; van Gunsteren, W. F. *Chem. Phys. Lett* **1994**, *6*, 529–539.

(45) Berg, B. A.; Neuhaus, T. *Phys. Rev. Lett.* **1992**, *68*, 9–12.

(46) Lee, J. *Phys. Rev. Lett.* **1993**, *71*, 211–214.

(47) Dayal, P.; Trebst, S.; Wessel, S.; Würtz, D.; Troyer, M.; Sabhapandit, S.; Coppersmith, S. N. *Phys. Rev. Lett.* **2004**, *92*, 097201.

(48) Escobedo, F. A.; Martinez-Veracoechea, F. J. *J. Chem. Phys* **2007**, *127*, 174103.

(49) Plimpton, S. *J. Comp. Phys.* **1995**, *117*, 1–19.

(50) Verlet, L. *Phys. Rev.* **1967**, *159*, 98–103.

(51) Martínez, L.; Andrade, R.; Birgin, E. G.; Martínez, J. M. *J. Comput. Chem.* **2009**, *30*, 2157–2164.

(52) J.Chang, C. *Fluid Phase Equilib.* **1992**, *15*, 235–242.

(53) Katritzky, A. R.; Oliferenko, A. A.; Oliferenko, P. V.; Petrukhin, R.; Tatham, D. B.; Maran, U.; Lomaka, A.; Acree, W. E. *J. Chem. Inf. Comput. Sci.* **2003**, *43*, 1794–1805.

(54) Mobley, D. L.; Gilson, M. K. *Annu. Rev. Biophys.* **2017**, *46*, 531–558.

(55) Abraham, M. H.; Whiting, G. S.; Fuchs, R.; Chambers, E. J. *J. Chem. Soc., Perkin Trans. 2* **1990**, 291–300.

(56) Rizzo, R. C.; Aynechi, T.; Case, D. A.; Kuntz, I. D. *J. Chem. Theory Comput.* **2006**, *2*, 128–139.

(57) Hadley, K. R.; McCabe, C. *J. Phys. Chem. B* **2010**, *114*, 4590–4599.

(58) Hadley, K. R.; McCabe, C. *Mol. Simul.* **2012**, *38*, 671681.